

# Superhumps in V348 Pup

Daniel J. Rolfe,<sup>1</sup> Carole A. Haswell,<sup>1</sup> and Joseph Patterson<sup>2</sup>

<sup>1</sup>Department of Physics and Astronomy, The Open University, Walton Hall, Milton Keynes MK7 6AA

<sup>2</sup>Department of Astronomy, Columbia University, 538 W. 120th St., New York, New York 10027

Accepted March 2000

## ABSTRACT

The eclipsing novalike cataclysmic variable star V348 Pup exhibits a persistent luminosity modulation with a period 6 per cent longer than its 2.44 hour orbital-period ( $P_{\text{orb}}$ ). This has been interpreted as a “positive superhump” resulting from a slowly precessing non-axisymmetric accretion disc gravitationally interacting with the secondary. We find a clear modulation of mid-eclipse times on the superhump period, which agrees well with the predictions of a simple precessing eccentric disc model. Our modelling shows that the disc light centre is on the far side of the disc from the donor star when the superhump reaches maximum light. This phasing suggests a link between superhumps in V348 Pup and late superhumps in SU UMa systems. Modelling of the full lightcurve and maximum entropy eclipse mapping both show that the disc emission is concentrated closer to the white dwarf at superhump maximum than at superhump minimum. We detect additional signals consistent with the beat periods between the implied disc precession period and both  $\frac{1}{2}P_{\text{orb}}$  and  $\frac{1}{3}P_{\text{orb}}$ .

**Key words:** accretion discs – binaries: close – binaries: eclipsing - stars: individual: V348 Pup – stars: cataclysmic variables

## 1 INTRODUCTION

V348 Pup (1H 0709–360, Pup 1) is a novalike cataclysmic variable (CV): a system with a high mass transfer rate which maintains its accretion disc in the hot, ionized, high viscosity state reached by dwarf novae in outburst. It exhibits deep eclipses in its optical and infrared lightcurves (Tuohy et al. 1990): it is a high inclination system with orbital period  $P_{\text{orb}} = 2.44$  hours (Baptista et al. 1996).

### 1.1 Superhumps

Modulations in luminosity with a period a few per cent longer than the orbital period have been observed in many short period CVs (see reviews in Molnar & Kobulnicky 1992, Warner 1995, Patterson 1998a). These modulations typically take the form of a distinct increase in luminosity, or superhump. The standard explanation of this phenomenon is that the system contains an eccentric precessing accretion disc.

If the accretion disc extends out far enough, the outermost orbits of disc matter can resonate with the tidal influence of the secondary star as it orbits the system. A 3:1 resonance can occur which results in the disc becoming distorted to form an eccentric non-axisymmetric shape. The tidal forces acting on this eccentric disc will cause it to precess slowly in a prograde direction.

The superhump period,  $P_{\text{sh}}$ , is then the beat period

between the disc precession period,  $P_{\text{prec}}$ , and the orbital period,  $P_{\text{orb}}$  (Osaki 1996):

$$\frac{1}{P_{\text{sh}}} = \frac{1}{P_{\text{orb}}} - \frac{1}{P_{\text{prec}}}.$$

$P_{\text{sh}}$  is the period on which the relative orientation of the line of centres of the two stars and the eccentric disc repeats. Possible models for the light modulation on  $P_{\text{sh}}$  are described below. This paper considers these models in relation to our observations.

In the tidal model the superhump is a result of tidal stresses acting on the precessing eccentric disc (Whitehurst 1998b). The light may be due to a perturbation of the velocity field in the outer disc, leading to azimuthal velocity gradients and crossing or converging particle trajectories. Thus extra dissipation modulated on the superhump period arises when the secondary sweeps past the eccentric disc. In addition, the superhump-modulated tidal stress would lead to a superhump-modulated angular momentum loss from the disc which would facilitate a variation in the mass transfer rate through the disc, and hence a modulation in disc luminosity.

The bright spot model arises from noting that the energy gained by material in the accretion stream will depend on how far it falls before impacting on the disc (Vogt 1981). The energy dissipated at impact will be modulated on the superhump period since the non-axisymmetric disc radius

causes a stream-disc impact region at varying depths in the white dwarf potential well.

Recent SPH simulations of accretions discs in AM CVn stars lead to a third, more realistic, model in which the disc shape changes from nearly circular to highly eccentric over the course of a superhump period (Simpson & Wood 1998). Superhumps arise from viscous energy production as the distorting disc is tidally stressed. Other SPH simulations (e.g. Murray 1996, 1998) also reveal a disc whose shape changes, with Murray (1996) predicting superhump modulations from both the periodic compression of the eccentric disc and the varying depth in the primary Roche potential at which the stream impacts the disc.

Dwarf novae in super-outburst exhibit two distinct positive superhump phenomena (Vogt 1983, Schoembs 1986). Normal superhumps appear early in the super-outburst and fade away towards the end of the outburst plateau to be replaced with ‘late’ superhumps which persist into quiescence. These late superhumps are roughly anti-phased with the normal superhumps, and are more likely to be analogous to the persistent superhumps seen in novalikes (Patterson 1998b), where the system has had sufficient time to settle into a steady state. Our extensive photometry (Section 2) reveals similarities between superhumps in V348 Pup and late superhumps in dwarf novae.

In Section 3.1 we present power spectra revealing the superhump period and additional signals close to orbital period harmonics. In Section 3.2 we estimate the orbital parameters,  $q$  and  $i$ , for V348 Pup using the average orbital lightcurve and the superhump period. The waveform of the superhump modulation is discussed in Section 3.3. Section 3.4 considers average orbital lightcurves grouped according to superhump phase. In Section 3.5 we fit our lightcurves with a precessing eccentric disc model, hence deducing the location of light centre of the disc. We consider the results of maximum entropy eclipse mapping in section 3.6. Our results and their implications are discussed in Section 4.

## 2 THE OBSERVATIONS

The observing campaign comprises 24 nights of rapid photometry from December 1991, February 1993 and January 1995 (see Table 1). The 1991 and 1993 observations (12 and 8 nights respectively) were taken using the the 40-inch telescope at CTIO with a blue copper sulphate filter. The January 1995 run consists of 4 nights of R band data. All the data have been corrected for atmospheric extinction and the 1995 data have also been calibrated to give an absolute flux. In 1995 the average out of eclipse R magnitude is 15.5 mag; at mid-eclipse  $R = 16.8$ . Examples of typical data are plotted in Figure 1.

## 3 ANALYSIS

We determined mid-eclipse timings as described in Section 3.5 from which we determined an orbital ephemeris for this dataset

$$T_{\text{mid}} = \text{HJD } 2448591.667969(85) + 0.101838931(14)E.$$

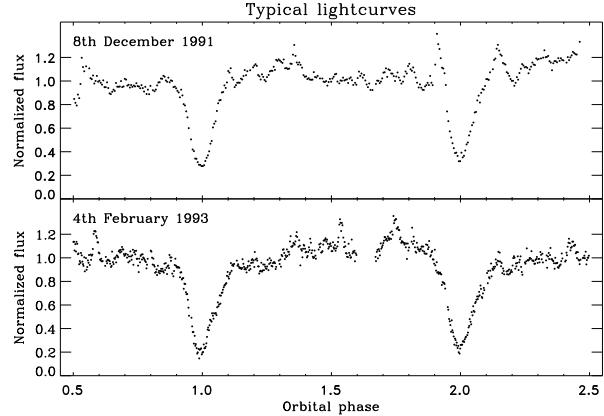


**Figure 1.** 4 cycles of typical data from 1991 and 1993.

**Table 1.** Log of observations

Date	HJD start -2440000	Duration (hours)	Integration time (sec)	Filter
1991 Dec 1	8591.6779	3.96	42	CuSO <sub>4</sub>
1991 Dec 2	8592.6138	3.55	42	CuSO <sub>4</sub>
1991 Dec 3	8593.6092	5.68	42	CuSO <sub>4</sub>
1991 Dec 4	8594.6249	5.14	42	CuSO <sub>4</sub>
1991 Dec 5	8595.6203	5.37	42	CuSO <sub>4</sub>
1991 Dec 6	8596.6328	5.18	42	CuSO <sub>4</sub>
1991 Dec 7	8597.6293	5.08	42	CuSO <sub>4</sub>
1991 Dec 8	8598.6107	5.59	42	CuSO <sub>4</sub>
1993 Feb 2	9020.5672	5.56	10	CuSO <sub>4</sub>
1993 Feb 3	9021.5549	6.24	10	CuSO <sub>4</sub>
1993 Feb 4	9022.5497	6.17	10	CuSO <sub>4</sub>
1993 Feb 9	9027.5565	3.71	10	CuSO <sub>4</sub>
1993 Feb 11	9029.7051	2.36	10	CuSO <sub>4</sub>
1993 Feb 12	9030.6851	2.84	10	CuSO <sub>4</sub>
1993 Feb 13	9031.5446	6.02	10	CuSO <sub>4</sub>
1993 Feb 14	9032.5427	6.23	10	CuSO <sub>4</sub>
1993 Feb 21	9039.6498	3.20	10	CuSO <sub>4</sub>
1993 Feb 22	9040.5572	3.13	10	CuSO <sub>4</sub>
1993 Feb 23	9041.5479	2.52	10	CuSO <sub>4</sub>
1995 Jan 3	9720.5689	4.83	10	R band
1995 Jan 4	9721.5521	3.32	10	R band
1995 Jan 5	9722.5509	7.15	10	R band
1995 Jan 6	9723.5472	7.24	10	R band

This is consistent with the Baptista et al. (1996) ephemeris within the quoted error limits. We adopt our ephemeris for this analysis. The eclipse timings are given in Table 2.

### 3.1 The superhump period

Before performing any analysis, we normalized each night of data by dividing by the average out of eclipse value.

To make detection of non-orbital modulations in the data easier, the average orbital lightcurves\* from each years’ observations were calculated and subtracted from the corresponding data. The resulting lightcurves contain no orbital

\* Superhump phase grouped average lightcurves are shown in Figure 7.

**Table 2.** Eclipse timings

HJD mid-eclipse -2440000	Error estimate	HJD mid-eclipse -2440000	Error estimate
December 1991		February 1993	
8591.769462	0.000121	9020.613001	0.000036
8592.686379	0.000096	9020.715111	0.000043
8593.705382	0.000120	9021.632451	0.000090
8593.806642	0.000017	9021.734218	0.000082
8594.722715	0.000090	9022.650034	0.000232
8594.824510	0.000162	9022.752227	0.000175
8595.640158	0.000104	9027.640565	0.000417
8595.742287	0.000201	9029.779356	0.000091
8596.657488	0.000082	9030.695522	0.000026
8596.759320	0.000100	9030.797304	0.000213
8597.676629	0.000068	9031.612099	0.000105
8597.778677	0.000083	9031.714122	0.000104
8598.694383	0.000058	9032.630438	0.000045
8598.796652	0.000090	9032.732446	0.000022
January 1995		9039.657734	0.000007
9720.653953	0.000003	9039.759941	0.000159
9720.756257	0.000300	9040.573722	0.000065
9721.571129	0.000069	9040.675596	0.000025
9721.672783	0.000132	9041.592531	0.000082
9722.589171	0.000043		
9722.690736	0.000053		
9723.607919	0.000087		
9723.709706	0.000135		
9723.811139	0.000068		

variations. Lomb-Scargle periodograms were calculated for each year's data, and are shown in Figures 2 and 3. The 1991 periodogram reveals a periodicity with period 0.10763 days and simple aliasing structure. The 1993 periodogram has higher resolution, more complicated alias structure, and the strongest periodicity at 0.10857 days. The 1995 power spectrum (having the least time coverage) is lower resolution, however a clear signal at 0.10760 days and its aliases is present. By comparison with the clearer 1991 and 1993 spectra we surmise the 0.10760-day peak is the true signal. These periods are all close to 6 per cent greater than  $P_{\text{orb}}$  and correspond to the period excesses,  $\epsilon$ , shown in Table 3, defined using superhump period,  $P_{\text{sh}} = (1+\epsilon)P_{\text{orb}}$ . The inferred disc precession periods are also shown in Table 3.

It is notoriously difficult to determine errors in periods measured from periodograms. To estimate the errors in the periods detected here, various fake datasets were generated. The lightcurves were smoothed and the residuals used to characterize the variance of the random noise. Various types of noise with the same variance were added to both the smoothed lightcurves and smoothed superhump modulations. The variance in the period value determined from these different datasets provides a measure of the error in the period measurement. Since the smoothed data will still contain noise artefacts these are probably underestimates. The 1993 dataset with its 20-day time base should provide the most precise period. Therefore, the possibility that the real 1991 and 1995 superhump periods are in fact closer to the 1993 value than our measurements suggest should not be ruled out, as Figure 3 shows. However, variability in the detected periodicity has also been seen before for superhumps (Patterson 1998b).

Superhumping systems show a clear correlation between

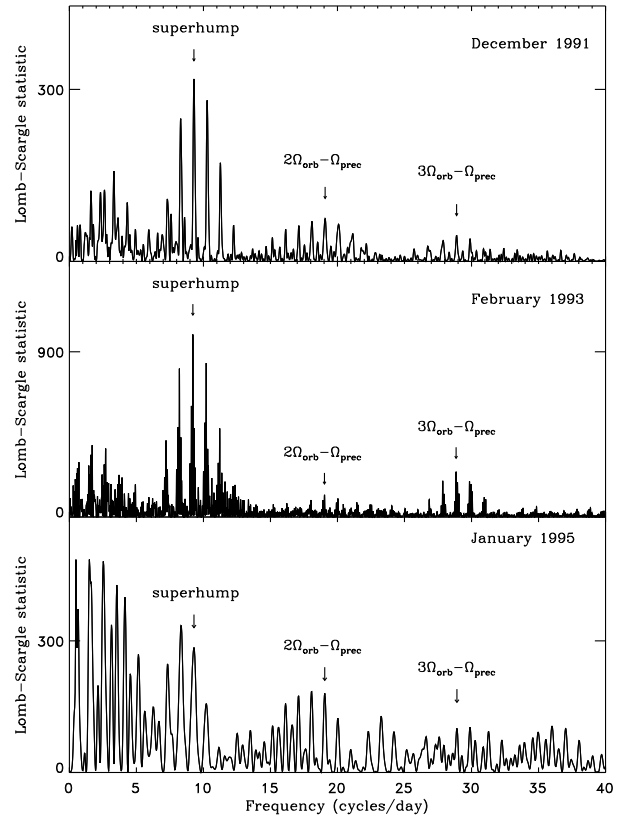


**Figure 2.** Power spectra. Arrows from left to right indicate the superhump period and the sidebands of the first and second harmonics of the orbital period (see Table 4).

$\epsilon$  and  $P_{\text{orb}}$ , with  $\epsilon$  increasing with  $P_{\text{orb}}$ ; the superhump periods we detect in V348 Pup are consistent with this trend (Figure 3, Patterson 1998b).

The power spectra also reveal signals at frequencies corresponding to sidebands of harmonics of the orbital period. The strongest such detections are at periods corresponding to  $2\Omega_{\text{orb}} - \Omega_{\text{prec}}$  and  $3\Omega_{\text{orb}} - \Omega_{\text{prec}}$  (marked with arrows in Figure 2): the predicted and the directly measured values of these sidebands are shown in Table 4, and graphically in Figure 4. The errors in these periods were estimated using the method described earlier. The detected periods do not all agree to within the estimated errors, suggesting that the error estimates may be a little too low, as expected; the highest quality 1993 data agrees best.

The simplest way to produce these sidebands is by modulating the brightness or visibility of the superhump with orbital phase. If we consider the orbital lightcurve as a sum of Fourier components with frequencies  $n\Omega_{\text{orb}}$ , then following the approach of Warner (1986) and Norton, Beardmore & Taylor (1996), the eclipse of the superhump light source will produce signals at frequencies  $(n+1)\Omega_{\text{orb}} - \Omega_{\text{prec}}$ . Signals at frequencies  $(n-1)\Omega_{\text{orb}} + \Omega_{\text{prec}}$  are also predicted but we find no evidence of these; perhaps they are nullified by other signals of the same frequency in antiphase. In Section 3.4 we present evidence for a correlation between superhump amplitude and orbital phase; this modulation of superhump amplitude with orbital phase could also lead to

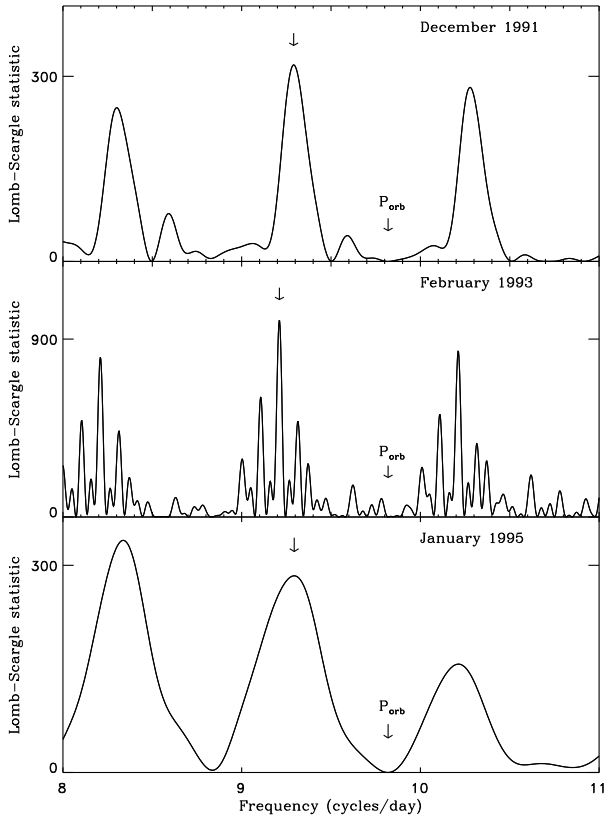


**Figure 3.** Detail of the power spectra shown in Figure 2. Arrows indicate the superhump period. The orbital period  $P_{\text{orb}}$  is also marked, from which it is clear that the orbital variation has been successfully removed.

**Table 3.** Measured superhump characteristics, period  $P_{\text{sh}}$ , the period excesses  $\epsilon$ , the inferred disc precession periods  $P_{\text{prec}}$  and the consequent estimates of the mass ratio  $q$ .

	$P_{\text{sh}}$ (d)	$\epsilon$	$P_{\text{prec}}$ (d)	Fractional amplitude	$q$
1991	0.107628(8)	0.0568	1.89	0.20	0.26
1993	0.108567(2)	0.0661	1.64	0.15	0.31
1995	0.10760(7)	0.0566	1.90	0.13	0.26

the observed sideband signals. The SPH models of Simpson & Wood (1998) predict the formation of double armed spiral density waves in the disc whose rotation rate, they suggest, might lead to observed signals at about three times the superhump frequency. They also suggest that viewing these structures from non-zero inclination could lead to the detection of further frequencies, although they do not make precise predictions. Observations of the dwarf nova IP Peg in outburst have revealed evidence of such spiral structure (Steeghs, Harlaftis & Horne 1997).

There is no significant signal around period  $P_{\text{prec}} = 1.6 - 1.9$  days in either the normalized or un-normalized lightcurves. The disc precession period is similarly absent in other persistently superhumping systems, notably AM CVn where  $P_{\text{prec}}$  is clearly revealed by absorption line spectroscopy (Patterson, Halpern and Shambrook 1993).

**Table 4.** Sidebands of the orbital period harmonics

	$\Omega = 2\Omega_{\text{orb}} - \Omega_{\text{prec}}$ Pred. P (d)	$\Omega = 2\Omega_{\text{orb}} - \Omega_{\text{prec}}$ Meas. P (d)	$\Omega = 3\Omega_{\text{orb}} - \Omega_{\text{prec}}$ Pred. P (d)	$\Omega = 3\Omega_{\text{orb}} - \Omega_{\text{prec}}$ Meas. P (d)
91	0.052327(1)	0.05241(1)	0.0345661(6)	0.034617(1)
93	0.0525477(4)	0.052540(1)	0.0346623(1)	0.03466(1)
95	0.05232(1)	0.052493(8)	0.034563(6)	0.034588(2)

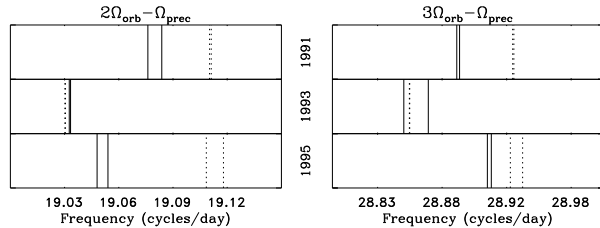


**Figure 4.** Sidebands of the orbital period harmonics. Dotted lines mark predicted frequency range for each signal, solid lines show the measured range.

### 3.2 The orbital parameters

The mass ratio,  $q$ , of a superhumper can be estimated, given its period excess,  $\epsilon$  (Patterson 1998b).

$$\epsilon = \frac{0.23q}{1 + 0.27q}.$$

This leads to the estimates of  $q$  for V348 Pup shown in Table 3. We favour the mass ratio,  $q = 0.31$ , estimated from the most accurate 1993 superhump period. We note that SPH simulations of eccentric discs (Murray 1998, 1999) suggest a more complicated relationship between  $\epsilon$  and  $q$  with the disc precession rate depending on the gas pressure and viscosity of the disc in addition to the mass ratio. This does not affect our substantive results.

If we assume that the secondary star is Roche lobe filling, the width,  $w$ , of eclipse of a point source at the centre of the compact object uniquely defines orbital inclination,  $i$ , as a function of  $q$ . We can thus compute  $i$  as a function of  $q$  and  $w$ .

When the centre of the compact object (point  $P$ ) is first eclipsed (orbital phase  $\phi_1$ ), about half of the disc area will be eclipsed, and therefore for a disc whose intensity distribution is symmetric about the line of centres of the two stars, the fraction of disc flux eclipsed at this phase will be  $\sim 0.5$  (Figure 5). Similarly at the end of the eclipse of  $P$  (orbital phase  $\phi_2$ ) the fraction of disc light visible is again  $\sim 0.5$ . Further assuming that the lightcurve consists purely of emission from a disc in the orbital plane, the full width of eclipse at half intensity will be equal to  $w$ .

Using the average eclipses from each of our datasets to give  $w$ , we obtained  $i$ . We checked the assumption that half of the disc area is eclipsed at  $\phi_1$  and  $\phi_2$ : for these values obtained it is a good assumption. We therefore adopt orbital parameters  $q = 0.31$ ,  $i = 81.1 \pm 1^\circ$ . The conclusions drawn later are identical to those obtained using  $q = 0.36$  with corresponding  $i = 80.0 \pm 1^\circ$  which resulted from an earlier estimate of  $q$ .

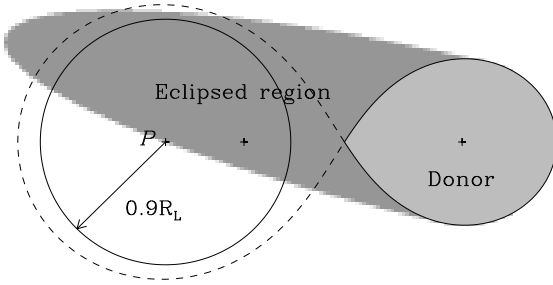


**Figure 5.** The eclipsed region of the orbital plane at phase  $\phi_1$  showing how approximately half of the area of a  $0.9R_L$  disc is eclipsed at this phase.

### 3.3 The superhump modulation

To define a zero point in superhump phase each set of data was folded onto its detected superhump period, binned into 100 phase bins, and a sine-wave was fitted to each (see Figure 6).

We assessed the contribution of flickering to these curves by using various methods of binning the data. Figure 6 shows the curves produced from simply averaging the points in each bin. Since flickering in the lightcurve consists of brief increases in luminosity, by giving more weight to the lower values in each bin or using only the lower points in a bin, the impact of flickering on these superhump phase binned lightcurves should be reduced. We therefore generated curves by averaging only the lowest 25 per cent of fluxes in each bin, and by weighting the lower values more strongly than the higher values. The curves produced by these different methods are virtually identical, except for a flux offset between each. This suggests that flickering has little effect on the superhump curves. Since we have extensive datasets and the timescales of the flickering and the superhumps are very different, this is not unexpected.

For a high inclination system a modulation on the superhump period will arise due to the eclipses of the precessing accretion disc changing as the disc orientation changes. This effect will occur in addition to the intrinsic variations in luminosity which are observed in non-eclipsing systems. Superhump modulations calculated using only non-eclipsing phases are almost identical to those in Figure 6, which implies that in this system the form of the superhump light curve is not affected by the changing eclipse shape.

The broad form of the modulation is consistent for all three sets of observations. The peak-to-peak fractional amplitudes are shown in Table 3 and decline steadily from year to year. The more detailed structure, particularly the region with lower flux between  $\phi_{sh} \sim 0.8$  and 1.0 in the 1991 modulation, appears to be genuine; we find neither flickering nor eclipses have significant effect. Furthermore the abrupt changes do not correspond to changes in system brightness from one night to the next.

Simpson & Wood (1998) calculate pseudo-lightcurves for superhumps. Assuming the light emitted from the disc is proportional to changes in the total internal energy of the gas in the disc, they present superhump shapes calculated for mass ratios of 0.050, 0.075 and 0.100 (their Figure 5). These curves have significant differences in morphology:

**Table 5.** Groups

Group	December 1991		February 1993		January 1995	
	$\frac{P_{\text{prec}}}{\phi_{sh}} = 1.89d$	$\sigma_\phi$	$\frac{P_{\text{prec}}}{\phi_{sh}} = 1.64d$	$\sigma_\phi$	$\frac{P_{\text{prec}}}{\phi_{sh}} = 1.90d$	$\sigma_\phi$
A	0.24	0.06	0.02	0.07	0.03	0.06
B	0.71	0.07	0.48	0.11	0.54	0.04

the  $q = 0.050$  curve has a sharp rise and slow decline, the  $q = 0.075$  curve is reasonably symmetric, and the  $q = 0.100$  curve has a slow rise and steeper decline. The cleanest and most reliable of our superhump curves, that from 1993, also shows an asymmetric shape, with a slow rise and sharper decline, agreeing best with their highest value of  $q = 0.100$ . We expect  $q \sim 0.31$  so this is encouraging.

### 3.4 Average lightcurves

Because of the sampling of our data (Table 1), the observed eclipses for each year appear in two rough groups, with superhump phases separated by about 0.5. We compared the average orbital lightcurves corresponding to each group. The average mid-eclipse superhump phase,  $\bar{\phi}_{sh}$ , of each group, and the range as indicated by the variance of  $\phi_{sh}$  for each group are shown in Table 5, the average orbital curves are shown in Figure 7.

The group A curve for 1991 (Figure 7a) displays a clear hump at orbital phase around -0.2: the mid-eclipse superhump phase of group A is 0.24, so eclipse should occur 0.25 in orbital phase after a superhump maximum. Group B has mid-eclipse superhump phase 0.71, meaning that the eclipse should occur around 0.3 in orbital phase before the superhump. The post-eclipse flux in group B is higher than in A, though the hump is not so sharp as in A.

Group A in the 1993 data displays a hump peaking just before mid-eclipse, while the curve for group B is rather flat out of eclipse. The mid-eclipse superhump phase of group A is 0.02, while group B has superhump phase 0.48. This is again consistent with the position of the superhump. The difference curve (i.e. A-B) seems to show a broad superhump which is partially eclipsed by the secondary. We expect group B to display a hump around orbital phase 0.5. This is not obvious, meaning that the superhump is more prominent when it occurs at orbital phase 0 (group A) than at phase 0.5. The superhump light is therefore not emitted isotropically<sup>†</sup>. Schoembs (1986) also noted a similar effect in OY Car. This will be considered further in Section 4.

The superhump phasing of the 1995 eclipses is almost the same as those observed in 1993, but the smaller extent of the 1995 data and the low fractional amplitude makes identifying the hump difficult without first subtracting the orbital light curve (compare Figs 6b and 6c). However, the flux during eclipse for group A is higher than for group B, consistent with the phasing which suggests that a superhump should occur at mid-eclipse.

<sup>†</sup> Eclipses of the superhump light will obviously be most important when the secondary is at inferior conjunction, i.e. when the superhump maximum is at orbital phase 0

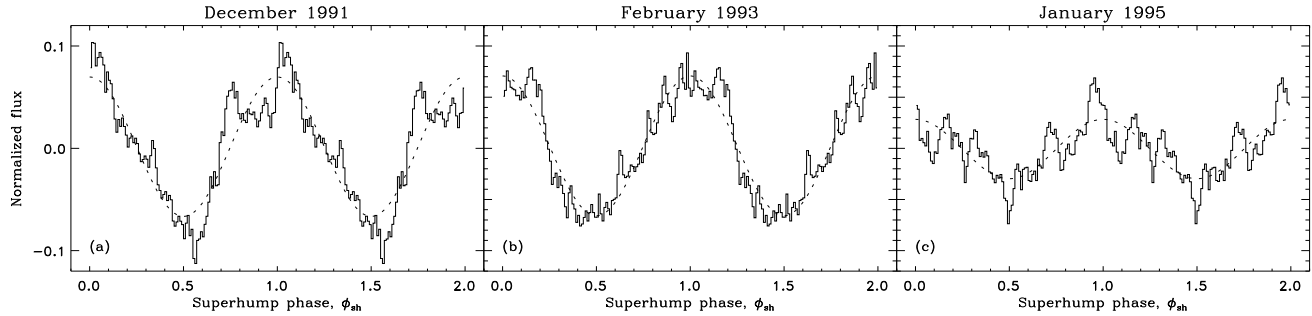


**Figure 6.** The superhump modulations. For each dataset, the average orbital light curve was subtracted and the resulting data folded and binned on superhump phase. Dotted lines show the sine waves fitted to determine phasing

### 3.5 Eclipse parameters

The O-C mid-eclipse times and the eclipse widths are shown in Figure 8. The mid-eclipse times were determined both by fitting a parabola to the deepest half of each eclipse and also by finding the centroid. The discrepancy between the two determinations provides an indication of the uncertainty.

As the eccentric disc precesses slowly in our frame, we expect to see the eclipse width and midpoint phase modulated on the apsidal precession period. These quantities will be similarly modulated in superhump phase, since the superhump phase and precession phase of an eclipse are both measures of the relative orientation of disc and secondary star at mid-eclipse. Figure 8 shows that eclipse timings for all years exhibit a precession period modulation. The widths also show evidence of a modulation. The limited superhump phase coverage means that conclusions cannot easily be drawn from inspecting the datapoints alone. Such variations in eclipse asymmetry have been observed in other superhumping systems e.g. OY Car (Schoembs 1986) and Z Cha (Warner and O'Donoghue 1988, Kuulkers et al. 1991). To further investigate the disc shape we produced a simple model which was then fitted to the observed lightcurves.

Our simple eccentric disc prescription has a circular inner boundary with radius  $r_{min}$ , centred on the white dwarf. The outer boundary is an ellipse of semi-major axis  $a_{max}$ , eccentricity  $e$ , with one focus also centred on the white dwarf. The disc brightness at distance  $r(\alpha)$  from the white dwarf at an angle  $\alpha$  to the semi-major axis is

$$S(\alpha) \propto \left( \frac{r(\alpha) - r_{min}}{r_{max}(\alpha) - r_{min}} + \frac{r_{min}}{a_{max}(1 - e) - r_{min}} \right)^{-n},$$

where  $r_{max}(\alpha)$  is the distance from the white dwarf to the outer disc boundary at orientation  $\alpha$ . Brightness contours are therefore circular at the inner boundary, smoothly changing to elliptical at the outer boundary. This form for  $S(\alpha)$  reduces to  $S \propto r^{-n}$  if the disc is circular. Our model is sensible for a tidally distorted disc, since the tidal influence of the secondary star is unimportant at the inner disc, so we expect a more or less circular inner disc.

In an inertial frame, the disc slowly precesses progradely with period  $P_{prec}$ . With respect to the corotating frame of the system, this disc then rotates retrogradely with period  $P_{sh}$ . Let the relative orientation of the line of apsides of the disc with the line of centres of the binary when superhump maximum occurs be  $\phi_{disc}$ . The structure of the disc in our

model is therefore described by five parameters :  $r_{min}$ ,  $a_{max}$ ,  $e$ ,  $n$  and  $\phi_{disc}$ . This model was chosen as the simplest way to model an eccentric precessing disc, with as few parameters as possible. A similar model was used by Patterson, Halpern & Shambrook (1993) to model the disc in AM CVn.

We generated synthetic lightcurves for eclipses of our model disc using the orbital parameters from Section 3.2. By varying the parameters of our model to minimize the reduced  $\chi^2$  of the fit, we obtained a best fit of our model to our lightcurves. The smoothed superhump was subtracted from the lightcurves before fitting the model in order to remove the intrinsic variation in the disc flux, enabling us to study the shape of the disc. In Section 3.4 we noted that the superhump is more visible for  $\phi_{sh} = 0$  at  $\phi_{orb} = 0$ , so ideally we should subtract a superhump modulation which takes account of this variation in superhump prominence, but insufficient sampling of the disc precession phase by our data prevents us from doing this.

The downhill simplex method for minimizing multidimensional functions was used (the AMOEBA routine from Press et al., 1996). Each orbit (centred on an eclipse) was allowed to have a different total disc flux and a different uneclipsed flux. This prevents the variation of  $\sim 10$  per cent in flux from one orbit to the next from interfering with the results, and allows for the possibility of a contribution to the lightcurve from regions never eclipsed by the secondary star. The errors in the fluxes were estimated as being  $\sigma\sqrt{flux}$  where  $\sigma$  is the square root of the variance of the flux between orbital phase 0.2 and 0.8. This estimate therefore includes the effect of flickering.

We used two methods to assess the robustness and accuracy of these fits. Monte-Carlo methods estimated the size of the region in parameter space which has a  $\sim 75$  per cent chance of containing the ‘true’ values of the parameters. To assess the uniqueness and robustness of each solution we carried out the fitting process 20 times for each model/data combination starting each fit with a different random initial simplex. The solution chosen is that with the lowest value of reduced  $\chi^2$ . Extreme outlier solutions are rejected and the variance in the parameters for the remaining solutions is a measure of the accuracy with which the AMOEBA routine converges to a unique solution. The errors quoted in Table 7 for each parameter are whichever is the greater of confidence region estimate or the variance in the parameter from the multiple fits. The parameters resulting from all the fits are shown in Table 7.  $R_L$  is the Eggleton radius of the primary

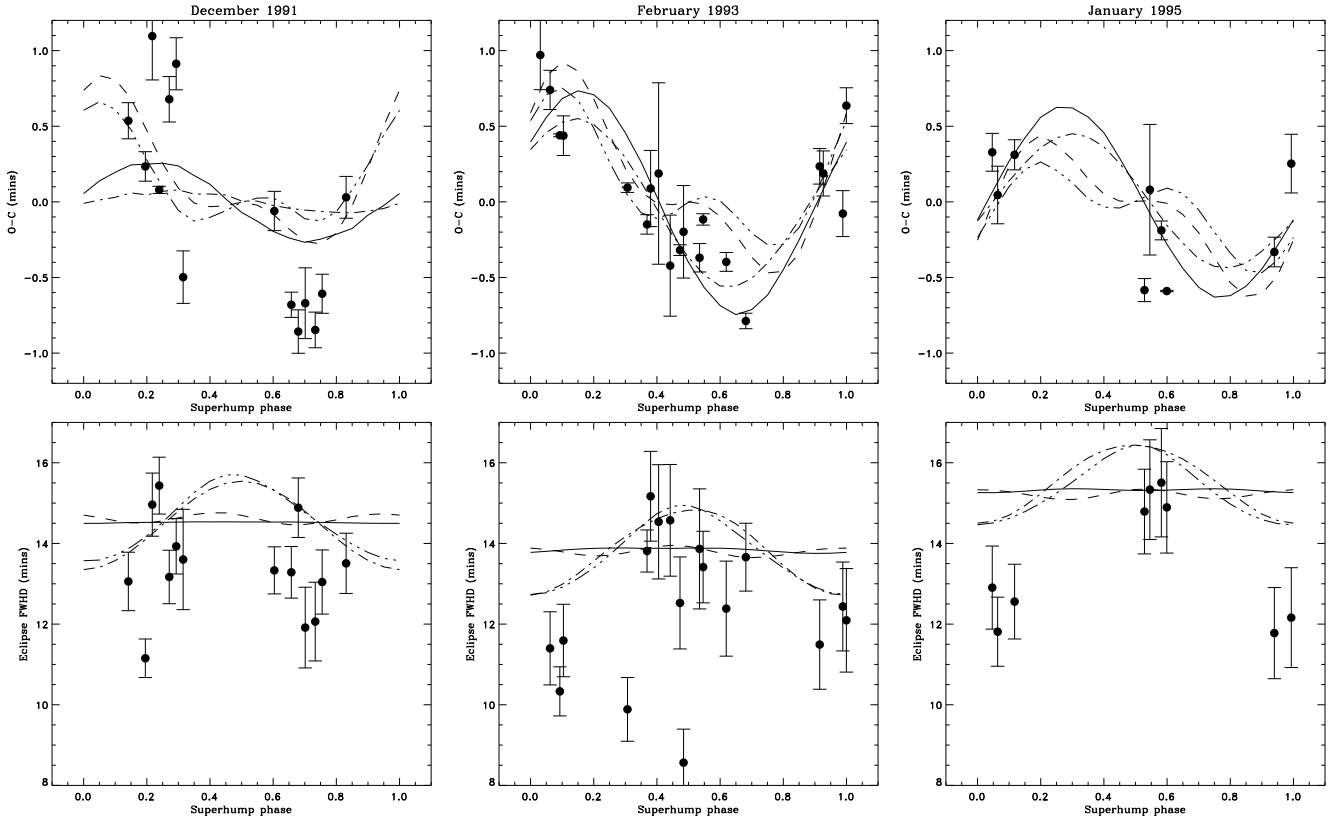


**Figure 8.** Eclipse parameters. The O-C mid-eclipse times and the full eclipse widths at half depth. The superhump phase,  $\phi_{sh}$ , is calculated using the superhump period,  $P_{sh}$  determined directly from the corresponding dataset. The continuous, dashed, dot-dashed and dot-dot-dot-dashed curves correspond to predictions from the lightcurve fits  $f$ ,  $e$ ,  $a$  and  $b$  described in Section 3.5.

Roche lobe (Eggleton 1983). The  $\chi^2$  surface in parameter space is not perfectly smooth. There is a broad global minimum superimposed with smaller amplitude bumps. Close to the global minimum the gradient of  $\chi^2$  is low and so small bumps can lead AMOEBA to settle into a local minimum near the real minimum.

Fits using the model as described above will be referred to as fit  $f$ . The emission extends out to 80 – 90 per cent of Roche lobe size, while the largest radius of the disc is  $a_{max}(1+e) = 0.97R_L$  for 1995 data. These results suggest that the disc does indeed extend out to the tidal cut-off radius,  $r_{tide}$ ;  $r_{tide} \sim 0.9R_L$  (Paczynski 1977).

The 1995 radius is 10 per cent larger than the 1991 and 1993 radii. The 1991 and 1993 observations are in blue CuSO<sub>4</sub> filter light, which should come from hotter inner disc regions; the 1995 observations are in R which is expected to weight the outer disc emission more heavily, perhaps causing the inferred disc radius to be largest for the 1995 observations. A simple model black-body disc with a  $T \propto R^{-\frac{3}{4}}$  temperature distribution, with  $T = 10,000K$  at the inner disc radius  $r_1 = 0.1R_L$  and with an outer disc radius  $r_2 = R_L$  was used to calculate eclipse profiles in the R and B band. Fitting model  $f$  to these eclipses showed no significant difference in outer disc radius between the R band and CuSO<sub>4</sub> filter fits.

The inner disc boundary and the index  $n$  in the flux distribution are poorly constrained. The eccentricity is robustly non-zero; the changing eclipse shape demands a non-axisymmetric disc.

The most interesting result is that all three datasets have  $\phi_{disc}$  around 0.4 to 0.5. This means that in our elliptical model the secondary star sweeps past the *smallest* radius part of the disc at superhump maximum – a result unexpected if tidal stressing of the disc by the gravitational influence of the secondary star is responsible for the superhump light. The implications of this result are discussed later.

We adjusted the model so that the eccentricity varied during the superhump cycle as  $e(\phi_{sh}) = e_0 \cos^2 \pi \phi_{sh}$ . This will be referred to as fit  $e$ . This variation in eccentricity follows Simpson & Wood's (1998) simulation in which the disc varies between being highly eccentric at the superhump maximum to almost circular away from the superhump. The results for  $r_{min}$  and  $a_{max}$  change very little, with  $a_{max}$  again larger in the red (1995) than the blue (1991 and 1993).  $\phi_{disc}$  is unchanged from fit  $f$  within the errors for all three years. The maximum eccentricity,  $e_0$ , is larger than when  $e$  was constant. This is expected since the eccentricity is demanded by the variation in O-C mid-eclipse times, and these O-C times are non-zero at times when  $e$  is less than  $e_0$ .

Next, we obtained fits in which the eccentricity was again constant, but where  $a_{max}$  was allowed to vary between  $a_1$  at superhump maximum to  $a_2$  half a superhump period later;  $a_{max}(\phi_{sh}) = a_1 + (a_2 - a_1) \sin^2 \pi \phi_{sh}$ . This will be referred to as fit  $a$ . This was an attempt to reproduce the observed variations in eclipse width (Figure 8).  $r_{min}$ ,  $e$  and  $\phi_{disc}$  are essentially the same as in the first fit, while the values of  $a_1$  and  $a_2$  imply a variation in  $a_{max}$  of ampli-

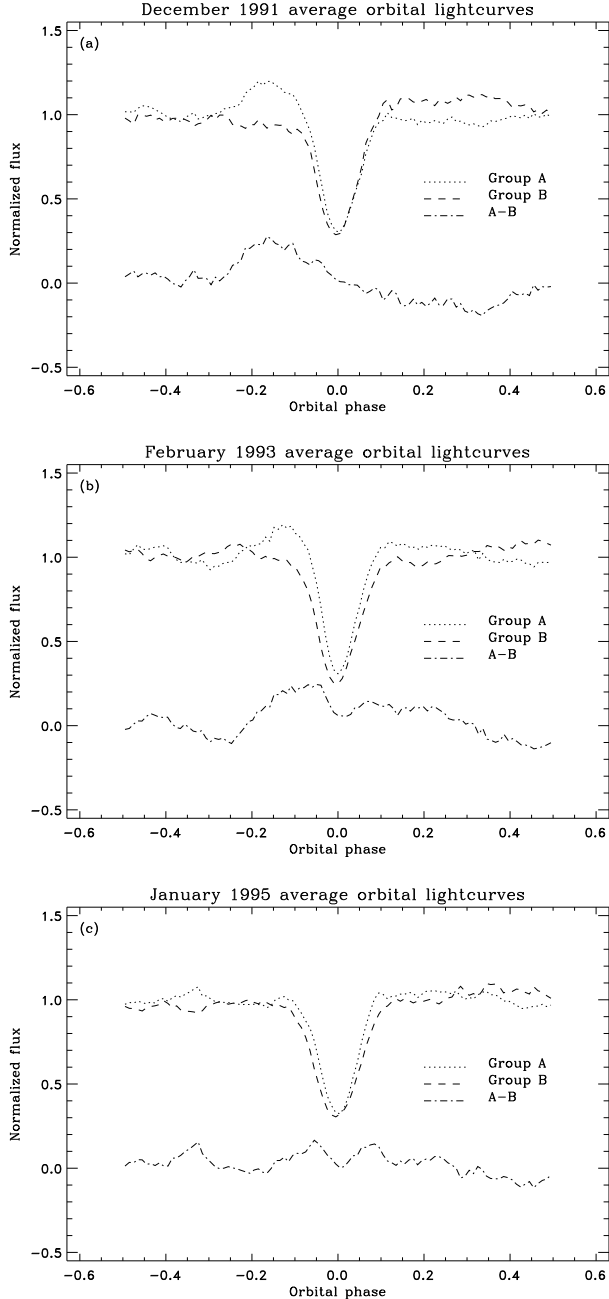


**Figure 7.** Average orbital lightcurves for each year. The data for each year are sorted into two groups, so that all eclipses in each group have mid-eclipse times with a similar superhump phase. The values of  $\phi_{sh}$  for each group are shown in Table 5. The third curve in each plot is the difference between the two lightcurves.

tude 20–25 per cent in the blue and 14 per cent in the red, with the disc being smallest at superhump maximum. At its largest, the disc extends to the edge of the Roche lobe. While these implied variations in disc size are large, they are comparable to the uncertainties in  $a_1$  and  $a_2$ , and so must be treated with caution.

The final variation on our model was to allow both  $e$  and  $a_{max}$  to vary as described above. This will be referred to as fit *b*. The eccentricity and  $\phi_{disc}$  are little different from

**Table 6.** Treatment of  $a_{max}$  and  $e$  in our four models.  $r_{min}$ ,  $n$  and  $\phi_{disc}$  are constant in all four models.

Fit	$a_{max}$	$e$
<i>f</i>	constant	constant
<i>e</i>	constant	$e_0 \cos^2 \pi \phi_{sh}$
<i>a</i>	$a_1 + (a_2 - a_1) \sin^2 \pi \phi_{sh}$	constant
<i>b</i>	$a_1 + (a_2 - a_1) \sin^2 \pi \phi_{sh}$	$e_0 \cos^2 \pi \phi_{sh}$

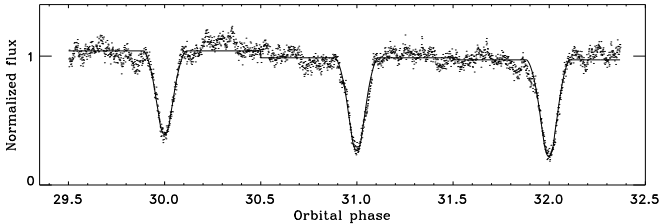


**Figure 9.** One night of the January 1995 data with the best fitting lightcurve using model *a* plotted as a continuous line. The discontinuities in the fit illustrate the different disc fluxes and uneclipsed fluxes allowed for each orbit. See Section 3.5.

the fits with  $e$  varying periodically and  $a_{max}$  constant, while the values of  $a_1$  and  $a_2$  follow those from the previous fit ( $e$  constant and  $a_{max}$  varying).

The treatment of  $a_{max}$  and  $e$  for each fit is summarized in Table 6. In Figure 9 we show part of the fit to the 1995 dataset using model *a*. The fit (shown as the continuous line) shows the different disc flux and uneclipsed flux allowed by our model in the form of the discontinuities at phase 30.5 and 31.5. The level of flickering out of eclipse can also clearly be seen, and was taken into account in our estimate of the errors as described above.

Formally, the best model is that which achieves the lowest value of reduced  $\chi^2$  ( $\chi_r^2$ ). In Figure 10 we show the values of  $\chi_r^2$  achieved for each model and dataset relative to the lowest. The minimum  $\chi_r^2$  achieved was around 0.8 for all datasets and models. This figure shows that the fits *a* and *b*, i.e. those in which  $a_{max}$  varies on the superhump cycle, produce significantly better fits to the 1993 and 1995 observations. The variation of  $e$  during the superhump cycle has little effect on the quality of these fits. There is less significant difference between the  $\chi^2$  achieved by the different fits to the 1991 observations, although allowing  $a_{max}$  or  $e$  to vary during the superhump cycle produces a better fit than when they are both constant. The significant reduction in  $\chi_r^2$  achieved by allowing  $a_{max}$  to vary implies that this model best represents the behaviour of the system.

It is also interesting to compare how well each model predicts the variation in the eclipse width and O-C mid-eclipse times. The predictions of each model are plotted in Figure 8. It is periodic variation in these two eclipse characteristics which requires the disc to be eccentric. The models poorly reproduce the O-C variations in the 1991 data. While the phasing of the predicted variation agrees with the observations, the amplitude is too low. The fits in which  $e$  varies during the superhump cycle predict a larger modulation in O-C times, a result of the larger eccentricity in these fits, but the agreement for these fits is still poor. The 1991 lightcurves suffer more from flickering than the 1993 and

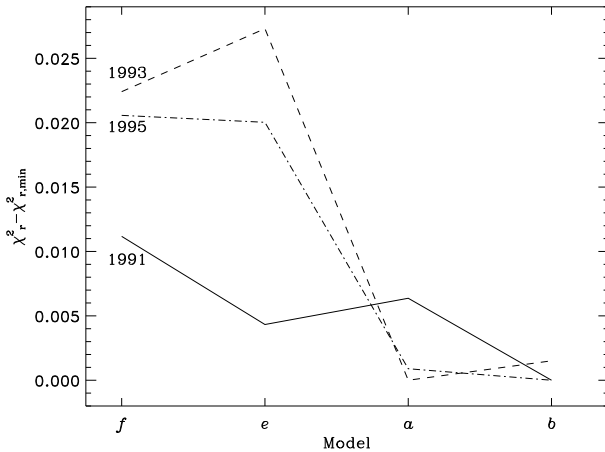


**Figure 10.** The minimum values of  $\chi^2$  achieved for the various models fitted (Section 3.5).

1995 data, with many eclipses distorted as a result. This is the most likely explanation for the poor agreement between our model and the 1991 lightcurves. The agreement between the predicted and observed O-Cs is very good for all models for the 1993 observations. The variation in eclipse width is only reasonably modelled by those fits in which  $a_{max}$  varies. The same is true of the 1995 fits.

The result of these comparisons between the different models, both the formal comparison of reduced  $\chi^2$  and the more subjective ‘chi-by-eye’ considerations of the O-C times and eclipse widths is that the models in which  $a_{max}$  varies during the superhump cycle predict the observations better than those in which  $a_{max}$  is constant.

All four models agree on three important points. The values of  $a_{max}$ ,  $a_1$  and  $a_2$  show that the disc is large, filling at least about 50 per cent of the Roche lobe area. The disc is not axisymmetric. From the consistent values of  $\phi_{disc}$  we see that when the superhump reaches maximum light, the light centre of the disc is on the far side of the white dwarf from the donor star.

### 3.6 Eclipse mapping

In Section 3.5 we used the changing eclipse profiles to constrain the parameters of a model intensity distribution. An alternative method for investigating the distribution of emission in the orbital plane is the commonly used eclipse mapping technique developed by Horne (1985). This method assumes that intensity distribution is fixed in the corotating frame of the binary, lies flat in the orbital plane and is constant. The surface of the secondary star is described by its Roche potential surface. Maximum entropy methods are used to obtain the intensity distribution by comparing the calculated lightcurve and observed lightcurves. The  $\chi^2$  statistic is used to ensure consistency between the observations and the fitted distribution, while the entropy is used to select the most appropriate solution from the multitude of possibilities. The entropy is usually defined such that the final solution is the smoothest or most axisymmetric map consistent with the observations. This technique has been

widely used, and O’Donoghue (1990) employed it to locate the source of the strong normal superhumps in Z Cha.

In order to study the shape of the precessing disc in V348 Pup, the PRIDA eclipse mapping code of Baptista & Steiner (1991) was modified so that the intensity distribution was fixed in the precessing disc frame rather than the corotating frame of the binary. Each year’s data was split into two groups (Section 3.4) but the lightcurves were not folded on orbital phase. This enabled us to obtain two maps for each year, corresponding to the groups given in Table 5. Since we expect the intensity distribution to change throughout the superhump cycle, grouping the eclipses as described means that the intensity distribution should be roughly the same for all eclipses in a group, an assumption of the eclipse mapping method. The superhump modulation was subtracted from each lightcurve as in Section 3.5. Normalization of the lightcurves was achieved by using the values for total disc flux and uneclipsed flux for each orbit obtained during the fitting procedure in Section 3.5. The uneclipsed flux was subtracted from each orbit and fluxes were then rescaled to produce an effective disc-only lightcurve. Various other normalization techniques were tested, and the detail of the reconstructed maps was sensitive to these changes. We used orbital parameters  $q = 0.31$  and  $i = 81^\circ$ , and looked for the most axisymmetric solution consistent with the data.

The most consistent result revealed by these eclipse maps is that the emission at superhump phase 0.5 is less centrally concentrated than at superhump phase 0. This is illustrated in Figure 11 which shows the maps for the two 1995 groups of eclipses. Figures 12a to 12c show the azimuthally averaged brightness distribution of each map. They show the flux at radius  $r$ ,  $F_r$ , multiplied by  $r$ ; this quantity is proportional to the total flux in an annulus at radius  $r$ . Figures 12b and 12c show how the disc extends further out at superhump phase 0.5 than at phase 0, while the curves in Figure 12a are both nearly the same, as expected since both of these curves show the situation roughly half way between superhump phase 0 and 0.5. This result is in agreement with the results of our fits of model  $a$  in which the disc size was allowed to change. These fits showed that the size of the emission region is larger at superhump phase 0.5 than at phase 0. The maps are asymmetric, but due to the sensitivity described above, we draw no conclusions from the detailed structure.

## 4 DISCUSSION

The phase of the superhump relative to the conjunction of the line of centres of the system and the semi-major axis of the disc should make it possible to determine whether the bright spot model or the tidal heating model better explains the source of the superhump. The simplest tidal model predicts that the superhump light should peak when (or slightly after) the largest radius part of the disc coincides with the line of centres. This is because the tidal interaction is strongly dependent on distance from the secondary, and so will be most significant in regions where the disc extends out close to the L1 point. However, if the bright spot model is to be believed, then the the superhump light source will be brightest when the accreting material has the furthest to

**Table 7.** Parameters resulting from fitting various models to the lightcurves (see Section 3.5). For the behaviour of  $a_{max}$  and  $e$  in each model see Table 6.

Fit	Year	$r_{min}/R_L$	$a_{max}/R_L$		$e$	$n$	$\phi_{disc}$
			$a_1/R_L$	$a_2/R_L$			
<i>f</i>	1991	0.13(13)		0.81(10)	0.035(03)	0.61(81)	0.46(17)
<i>f</i>	1993	0.12(09)		0.83(07)	0.106(02)	0.94(65)	0.41(11)
<i>f</i>	1995	0.11(13)		0.90(09)	0.082(03)	0.64(71)	0.53(13)
<i>e</i>	1991	0.13(10)		0.82(08)	0.121(06)	0.62(76)	0.35(15)
<i>e</i>	1993	0.09(10)		0.81(07)	0.144(03)	0.67(60)	0.41(03)
<i>e</i>	1995	0.08(10)		0.88(06)	0.102(04)	0.48(52)	0.55(15)
<i>a</i>	1991	0.12(14)	0.72(12)	0.88(17)	0.029(02)	0.59(84)	0.51(22)
<i>a</i>	1993	0.11(11)	0.76(08)	0.99(16)	0.099(04)	1.11(73)	0.41(15)
<i>a</i>	1995	0.10(16)	0.78(11)	0.91(09)	0.068(05)	0.34(96)	0.53(21)
<i>b</i>	1991	0.12(15)	0.74(09)	0.89(20)	0.104(08)	0.55(79)	0.35(18)
<i>b</i>	1993	0.10(09)	0.76(08)	0.98(13)	0.140(05)	0.99(61)	0.41(12)
<i>b</i>	1995	0.09(17)	0.80(09)	0.93(10)	0.084(06)	0.42(61)	0.56(22)

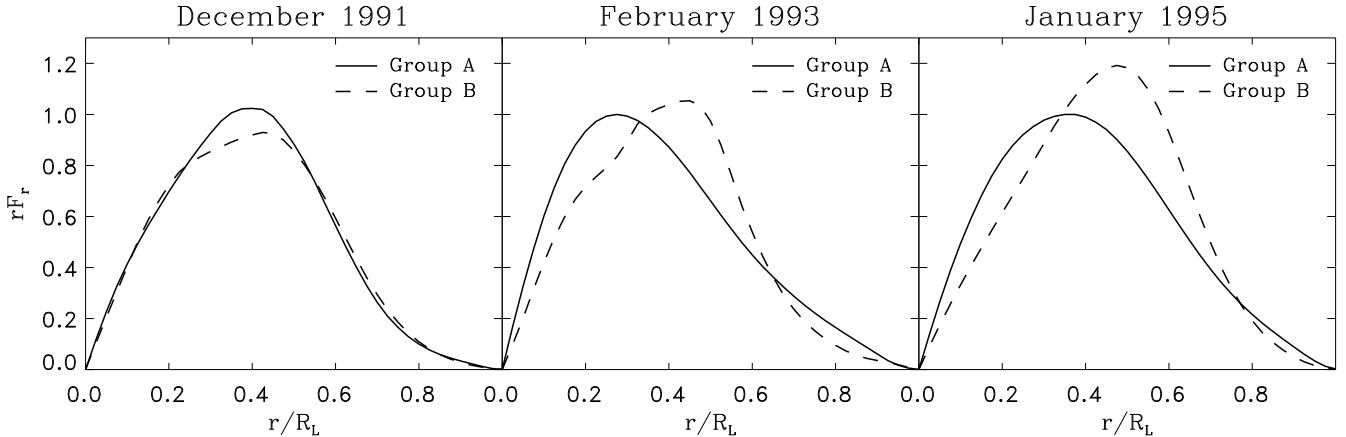


**Figure 12.** Azimuthally averaged flux in maximum entropy eclipse maps. Quantity plotted,  $rFr$ , is proportional to flux in annulus at radius  $r$ . See Section 3.6.

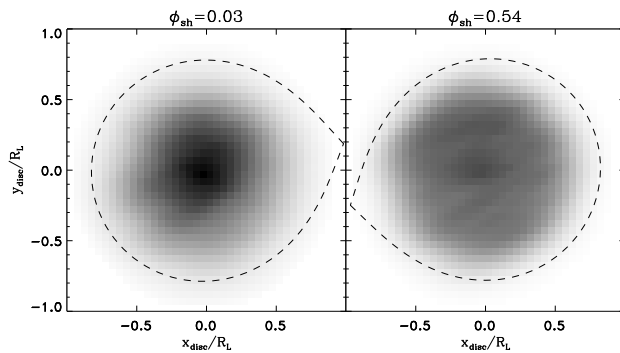


**Figure 11.** Maximum entropy eclipse maps of the intensity distribution in the *precessing* frame of the disc from the 1995 data. The *average* orientation of the primary Roche lobe for each group is also shown. See Section 3.6. The grey scale is the same for both maps.

fall. In other words, the superhump should occur when the stream impacts on the disc at its smallest radius.

The mid-eclipse times shown in the top row of panels in Figure 8 show the eclipses to be earliest around superhump phase 0.75 in all cases. Assuming that the centre of light of the eccentric disc is offset from the white dwarf in the direction of the largest radius, we can deduce the disc orientation during these eclipses to be as shown in Figure 13a. A quarter of a superhump period later, the orientation of the disc has barely changed, the secondary will be lined up with the smallest radius part of the disc and the superhump phase will be 0.0 (Figure 13b). Therefore superhump maximum occurs when the secondary star is lined up with the smallest radius part of the disc. The values of  $\phi_{disc}$  in Table 7 agree with this deduction. This phasing is consistent with the bright spot model for the superhump emission but is inconsistent with the simple tidal heating model. In Section 3.4, we noted that the superhump light appears not to be emitted isotropically: the superhump is strongest when it occurs around orbital phase 0. This is easily explained if the major contribution to superhump light is the bright spot: the bright spot is most visible when it is on the nearside of the accretion disc. Schoembs (1986) observed late super-

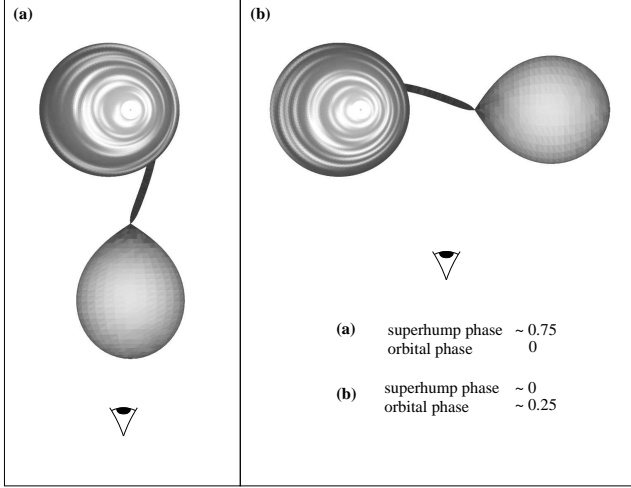


**Figure 13.** The first row of Figure 8 shows the eclipses to be earliest at superhump phase  $\phi_{\text{sh}} \sim 0.75$ , which implies orientation (a), from which we deduce the relative phasing of disc and secondary star at superhump maximum ( $\phi_{\text{sh}} = 0$ ) shown in (b).

humps in the eclipsing SU UMa dwarf nova OY Car, also a high inclination system. When a superhump was coincident with a pre-eclipse orbital hump, the combined amplitude was greater than that predicted for a linear superposition of the individual amplitudes i.e. OY Car's late superhumps were strongest around orbital phase 0. However, van der Woerd et al. (1988) studied the dwarf nova VW Hyi, concluding that there was no correlation between the orbital phase and amplitude of late superhumps. Since VW Hyi has an intermediate inclination,  $\sim 60^\circ$  (Schoembs & Vogt 1981), the bright spot visibility need not vary with phase, so if the bright spot is the main superhump light source we expect no variation in superhump amplitude with orbital phase.

Krzeminski & Vogt (1985) studied OY Car during a super-outburst and through variations in the O-C eclipse timings deduced the presence of an eccentric disc with phasing similar to that in V348 Pup. Krzeminski & Vogt's definition of O-C time was criticized by Naylor et al. (1987), with Naylor et al. concluding that the O-C evidence was weaker than originally thought.

Schoembs (1986) followed OY Car from early in a super-outburst almost until the return to quiescence, observing the  $\sim 180^\circ$  phase change from normal superhumps around the height of the outburst to late superhumps during the decline of the super-outburst. Patterson et al. (1995) observed the same change in superhump phase late in a super-outburst of V1159 Ori. Hessman et al. (1992) studied OY Car at the end of a super-outburst. By looking at the varying hot spot eclipse ingress times, and considering the trajectory of the accretion stream, they concluded that the disc was eccentric. The orientation of the disc at superhump maximum was very similar to that which we find in V348 Pup.

The broad waveform of these late superhumps in OY Car (Hessman et al.) was also similar to the superhump modulation in V348 Pup. Such similarity between late superhumps in OY Car and the superhumps in V348 Pup is not surprising. Late superhumps in dwarf novae appear towards the end of the superoutburst, after the disc has had time to adjust to its high state. V348 Pup is persistently in a

high state. Superhumps in a novalike system might resemble those to which the superhumps in a superoutbursting dwarf nova would tend if it remained in superoutburst for a long time. It seems likely that the mechanism responsible for late superhumps in SU UMa systems is the same mechanism responsible for superhumps in V348 Pup. However, Skillman et al. (1998) observed strong superhumps in the nova-like TT Ari throughout 1997 whose waveform is triangular like those of normal superhumps in dwarf novae.

There are many other studies of the disc structure in SU UMa stars during superoutburst. Vogt (1981) and Honey et al. (1988) found evidence for an eccentric precessing disc in Z Cha from the radial velocity variations of various absorption and emission lines respectively. The very prominent normal superhump in Z Cha made it possible for Warner & O'Donoghue (1988) to study the location of the superhump light source. They found strong departures from axisymmetry in the superhump surface-brightness. O'Donoghue (1990) employed a modified eclipse mapping technique to Z Cha lightcurves and found the normal superhump light coming from three bright regions of the disc rim, located near the L1 point and the leading and trailing edges of the disc, concluding that the superhumps are tidal in origin, and that a highly eccentric disc with a smooth brightness distribution is not necessary to explain superhump behaviour. One anomalous eclipse did confine the superhump light source in Z Cha to the region of the quiescent bright spot. van der Woerd et al. (1988) concluded that the late superhumps in VW Hyi come from an optically thin plasma and could be a result of tidal interaction.

In the SPH simulations of Murray (1996, 1998) pseudo-lightcurves are produced by assuming the heat produced by viscous dissipation to be radiated away where it is generated. Murray (1996, 1998) reveals an extended superhump light source in the outer disc, while Murray (1996) reveals an additional superhump modulation which arises from the impact of the accretion stream with the edge of the disc occurring at a varying depth in the primary Roche potential. This additional weaker superhump modulation is approximately  $180^\circ$  out of phase with the modulation due to tidal stressing, another similarity between late superhumps in dwarf novae, the persistent superhumps in V348 Pup and the bright spot model.

If we consider the stream to impact the disc at radius  $r$  in a  $\frac{1}{r}$  potential, then the luminosity,  $L$ , of the bright spot should vary roughly as  $\Delta(\frac{1}{r})$ . Considering the change in  $r$  as the disc with eccentricity  $e$  precesses, we get  $\frac{\Delta L}{L} \sim 2e$ . The eccentricities we find are in the range 0.035–0.15 predicting superhump fractional amplitude in the range 0.07–0.3. This is consistent with the measured superhump amplitudes in V348 Pup (Table 3).

While we limit the conclusions drawn from our eclipse maps in Section 3.6, there are a number of points deserving consideration.

Our eclipse maps do not show evidence of a bright spot, but this does not rule out the possibility that a bright spot is the source of the superhump light, for the following reasons. First, we subtracted the superhump modulation from the lightcurves before performing the eclipse mapping, which should reduce the contribution of the bright spot in the maps if it is the primary source of the superhump light. Also, our maps are fixed in the precessing disc frame, rather than

the orbital frame of the system, so the hot spot should be blurred azimuthally in our maps by  $\sim 70^\circ$  corresponding to the eclipse width of the system of  $\sim 0.2$  in orbital phase. There will be additional azimuthal blurring since the eclipses contributing to each map have a spread of disc orientations at mid-eclipse corresponding to the values of  $\sigma_\phi$  in Table 5. Azimuthal structure in the maps is also suppressed by looking for the maximally axisymmetric solution.

The eclipse maps tell us that the azimuthally averaged radial extent of the emission is lowest at superhump maximum, shown in Figure 12. If this change in extent of the emission region is interpreted as a result of a changing disc size, the the smaller disc radius at superhump maximum is consistent with the bright spot model for the superhump light source.

In the SPH models of Simpson & Wood (1998), the symmetry axis of the disc is aligned roughly perpendicular to the line of centres of the system when the superhump reaches maximum intensity. Inspecting their plots suggests that this model would lead to eclipses being earliest and widest at superhump phase 0 contrary to our findings. Simpson & Wood stress that their pseudo-lightcurves should be treated cautiously since no radiative processes were explicitly considered. The difference in the mass ratio between V348 Pup and the values considered in Simpson & Wood's simulations may affect the phasing of the early eclipses and superhump maximum, given that the predicted superhump waveform is sensitive to  $q$ . Furthermore, the spiral density waves in their simulations complicate the structure, so that simulated maps of the intensity may in fact produce reasonable agreement with our findings.

SPH simulations (Murray 1996 & 1998, Simpson & Wood 1998) show the behaviour of tidally distorted discs to be more complicated than a simple eccentric disc, and with treatment of radiative processes the predictions are likely to become even more complicated. Once such models are developed further, comparisons with observation should provide a more complete understanding of superhump phenomena.

## 5 SUMMARY

The eclipsing novalike cataclysmic variable V348 Pup exhibits positive superhumps. The period of these superhumps is in agreement with the generally observed  $\epsilon - P_{\text{orb}}$  relation for superhumpers.

Using the relation for  $q$  as a function of the superhump period excess,  $\epsilon$ , (Patterson 1998b) we estimate  $q = 0.31$ . Using the eclipse width we then estimate an orbital inclination of  $i = 81.1^\circ \pm 1^\circ$ .

Variations in the O-C mid-eclipse times and eclipse widths strongly suggest that V348 Pup harbours a precessing eccentric disc. We quantify this conclusion by fitting an eccentric disc model to the lightcurves. The relative orientation of the disc and secondary star at superhump maximum is more easily explained by the bright spot model for the superhump light source than the tidal heating model. A correlation between the amplitude and orbital phase of the superhumps is also more easily explained by the bright spot model.

Additional signals are detected at frequencies close to harmonics of the orbital frequency. The source of these vari-

ations is currently without conclusive explanation, but they could result from rotationally symmetrical structure in the disc, such as spiral waves, which have been predicted in simulations (e.g. Simpson & Wood 1998), and directly observed in the dwarf nova IP Peg (Steeghs, Harlaftis and Horne 1997). They may be a result of the correlation between superhump amplitude and orbital phase. In a high inclination system like V348 Pup the eclipse of the superhump light source may also explain these signals.

The phasing of the superhumps in V348 Pup is like that of late superhumps detected at the end of superoutbursts in SU UMa systems such as OY Car and VW Hyi (Schoembs 1986 and van der Woerd et al. 1988). The broad form of the superhump and the link between superhump amplitude and orbital phase are also similar to late superhumps in OY Car. By identifying the superhump mechanism in novalikes we are likely to also understand the mechanism for late superhumps in SU UMa systems. It is possible that this mechanism could be different from that which produces common superhumps, generally accepted to be a result of tidal stresses acting on an eccentric disc (O'Donoghue 1990).

## ACKNOWLEDGMENTS

The authors acknowledge the data analysis facilities at the Open University provided by the OU research committee and at the University of Sussex provided by the Starlink Project which is run by CCLRC on behalf of PPARC. The OU computer support provided by Chris Wigglesworth and compiling assistance from Sven Bräutigam is also much appreciated. The PRIDA eclipse mapping software (Baptista & Steiner 1991) was used courtesy of Raymundo Baptista. DJR thanks Rob Hynes for being a mine of useful advice and information. We thank Eugene Thomas and Jessica Zimmermann who carried out parts of the observation, and the support staff at CTIO for their sterling work. CAH thanks the Nuffield Foundation and the Leverhulme Trust for support. DJR is supported by a PPARC studentship.

## REFERENCES

- Baptista R., Steiner J. E., 1991, A&A, 249, 284
- Baptista R., Patterson J., O'Donoghue D., Buckley D., Jablonski F., Augusteijn T., Dillon W., 1996, IAUC, 6327
- Eggleton P.P., 1983, ApJ, 268, 368
- Hessman F.V., Mantel K.-H., Barwig H., Schoembs R., 1992, A&A, 263, 147
- Honey W.B., Charles P.A., Whitehurst R., Barret P.E., Smale A.P., 1988, MNRAS, 231, 1
- Horne K., 1985, MNRAS, 213, 129
- Krzeminski W., Vogt N., 1985, A&A, 144, 124
- Kuulkers E., van Amerongen N., van Paradijs J., Röttgering H., 1991, A&A, 252, 605
- Molnar L.A., Kobulnicky H.A., 1992, ApJ, 392, 678
- Murray J.R., 1996, MNRAS, 279, 402
- Murray J.R., 1998, MNRAS, 297, 323
- Murray J.R., 1999, astro-ph/9911466
- Naylor T., Charles P.A., Hassal B.J.M., Bath G.T., Berriman G., Warner B., Bailey J., Reinsch K., 1987, MNRAS, 229, 183
- Norton A.J., Beardmore A.P., Taylor P., 1996, MNRAS, 280, 937
- O'Donoghue D., 1990, MNRAS, 246, 29
- Osaki Y., 1996, PASP, 108, 39

Paczynski B., 1977, *ApJ*, 216, 822  
 Patterson J., Jablonski F., Koen C., O'Donoghue D., Skillman D.R., 1995, *PASP*, 107, 1183  
 Patterson J., 1998a, Disk-Instability Workshop, Kyoto, Japan  
 Patterson J., 1998b, *PASP*, 110, 1132  
 Patterson J., Halpern J., Shambrook A., 1993, *ApJ*, 419, 803  
 Press W.H., Teukolsky S.A., Vetterling W.T., Flannery B.P., 1992, *Numerical Recipes in C*, Cambridge University Press  
 Schoembs R., 1986, *A&A*, 158, 233  
 Schoembs R., Vogt N., 1981, *A&A*, 97, 185  
 Simpson J.C., Wood M.A., 1998, *ApJ*, 506, 360  
 Skillman D.R., Harvey D.A., Patterson J., Kemp J., Jensen L., Fried R.E., Garradd G., Gunn J., van Zyl L., Kiyota S., Retter A., Vannunster T., Warhurst P., 1998, *ApJ*, 503, L67  
 Steeghs D., Harlaftis R.T., Horne K., 1997, *MNRAS*, 290, L28  
 Tuohy I.R., Remillard R.J., Brissenden R.J.V., Bradt H.V., 1990, *ApJ*, 359, 204  
 van der Woerd H., van der Klis M., van Paradijs J., Beuermann K., Motch C., 1988, *ApJ*, 330, 911  
 Vogt N., 1981, *ApJ*, 252, 653  
 Warner B., 1986, *MNRAS*, 219, 347  
 Warner B., 1995, *Cataclysmic Variable Stars*, Cambridge University Press, Cambridge  
 Warner B., O'Donoghue D., 1988, *MNRAS*, 233, 705  
 Whitehurst R., 1988a, *MNRAS*, 213, 129  
 Whitehurst R., 1988b, *MNRAS*, 232, 35